PCCP

Accepted Manuscript

ROYAL SOCIETY OF CHEMISTRY

www.rsc.org/pccp

PCCP

RSCPublishing

ARTICLE

Phase separation induced shell thickness variations in the Electrospun Hollow Bioglass 45S5 Fiber mats for Drug Delivery Applications

D. Durgalakshmi and S. Balakumar*

Cite this: DOI: 10.1039/x0xx00000x

Received 00th January 2012,
Accepted 00th January 2012

DOI: 10.1039/x0xx00000x

www.rsc.org/

In the present work, sub micron sized hollow Bioglass 45S5 nanofibers are synthesised using electrospinning technique with the assistance of Poly vinyl pyrolidone polymer. The electrospinning process parameters are optimized to obtain reproducible nanofibers. The effect of solvent concentration and polymer concentrations affecting the morphology and formation of fibers. Ethanol and water is taken as source of concentration variant and the increase in the water dilution decreases the shell thickness of the hollow fibers. The mechanism of formation of hollow fibers is due to the phase separation occurs during physical cooling of the fibers. The equal ratio of ethanol and water diluted sol prepared fibers is showing higher performance in drug loading and releasing kinetics due to its narrow and linear size distribution. This fiber is also highly suitable for bone tissue engineering applications due to its linear fibrous 3D structural mat formation and suitable for large size scaling.

1. Introduction

Tissue engineering emerged as a promising alternative for the reconstitution of lost or damaged organs and tissues.[1] The biologically functional scaffolds play a critical role in the tissue engineering process, provide a 3D structure for cellular functions such as attachment, migration proliferation, differentiation and also serve as a vehicle for delivery of cells to the implant site.[2] The success of this process is determined by the biological and functional similarity of an engineered tissue with the native tissue.[3] Due to the unique properties and favourable cell behaviour of sub-micrometric bone features, such as in collagen fibrils towards fiber matrices, different fiber matrices were developed for bone tissue engineering applications.[4]

Bioactive glasses are considered as the first expression of bioactive ceramics, due to its high bioactivity level and their brittleness. These materials find clinical applications in those cases where high tissue regeneration is required without supporting high loads or stresses.[4] The apatite formation on the surface of bioactive glasses is calcium-deficient, carbonate-containing, nanocrystalline and therefore very similar to the biological ones. On the various types of Bioglass systems, Bioglass 45S5 is proved as highly bioactive and it can bond with both bone and tissue.[5a-b]

Recent development in the use of an electrospinning technique for tissue engineering scaffolds to create fibrous scaffold of biodegradable polymers is alarmingly exciting.[6] This technique is also being applied in the formation of fibers with submicron or nanoscale diameters and to form Nanofibrous scaffolds of bioactive glass. Due to their high surface area, bioactive glass nanofibers degrade rapidly and convert to hydroxyl carbonate apatite (HCA).[7] It was reported that the narrow sintering window of Bioglass 45S5 makes it difficult to produce fibers by the conventional melt – spinning methods without the glass crystallizing and that can be produced by the laser spinning method.[8] However, Bioglass fibers with diameters in the micron to submicron range, prepared from a melt-derived glass, are available commercially.[8-9] Literature on Bioglass fibers by electrospun technique is available only for the 70S30C glass system, which bonds only to bone and not with the tissue.[9-10] Zhao et al. reported that the porosity in the Bioglass matrices and their surface area accelerate the apatite deposition and the electrospun 70S30C glass fibers were solid and lack porosity in the fiber textures.[11]

In the present work, Bioglass 45S5 fibers have been fabricated using the sol-gel assisted electrospinning technique. The parameters such as polymer content, distance between needle and target, feeding rate, applied voltage, dilution condition altered the morphology, yield and surface area of the fibers that are analyzed in detail. The fibers were optimized to be porous, which is advantageous for adsorbing bone marrow aspirate, drug and growth factor delivery applications.

2. Experimental Section

2.1. Chemicals

Calcium nitrate tetrahydrate, Sodium hydroxide, Tetra ethyl ortho silicate (TEOS) and Orthophosphoric acid were procured from Alfa Aesar, India and used as precursors for the synthesis of Bioglass 45S5 (46.13 mol% SiO_2, 26.92 mol% CaO, 24.35 mol % Na_2O and 2.6 mol% P_2O_5). Polyvinyl pyrolidone (PVP) with the molecular weight of 13,00,000 was procured from Alfa Aesar, India and used to increase the viscosity of the Bioglass solution.

2.2. Synthesis Methods

The initial procedure involves mixing of Ethanol and water in the ratio of 1:1 with the addition of 1M HCl as a catalytic agent. The following reagents were added as per the molar ratio, in the order of calcium nitrate, orthophosphoric acid, TEOS and PVP (10 wt%). The solution was stirred for an additional 24 h and the resultant product was a transparent gel (Figure S1) and this is maintained as a stock solution at room temperature. At the time of the experiment, 5 ml of the stock was diluted with equal volumes of water, ethanol and water/ethanol (ratio of 1:1), the weighed mol% NaCl was added and stirred to get a homogeneous solution. The final solution was loaded to the electrospinning set up Espun nano, Physics Equipments Co., India for obtaining the fibers. The parameters such as polymer content in the Bioglass solution, distance between needle and target, feeding rate, applied voltage and final dilution medium were varied to obtain the beaded free hollow sub-micrometric fibers.

2.3. Instrumentations

The phase analysis of the sintered samples were investigated by X-ray diffraction (XRD) analysis with X-ray diffractometer (PANalytic, The Netherlands) using monochromatic Cu Kα (λ = 1.5405 Å) with the 2θ range from 10° to 80° at scanning speed of 0.5°/min. The oxidation state of the samples with respect to the sample composition was characterized using X-ray photoelectron spectroscopy (XPS) (Omicron Nanotechnology, Germany).

The phase analysis of the nanocomposites was analyzed using FTIR analyser using KBr as a standard reference and the spectra were collected in the wave number range 4000 to 400 cm^{-1}. The surface morphology and elemental analysis were examined by Field emission scanning electron microscopy (FESEM; Hitachi SU6600, Singapore). The samples were coated with gold using ion sputtering techniques at atmospheric pressure of 10 Kg/m^3 for 7 s in order to amplify the secondary electron signal. N_2 adsorption experiment were conducted using Micrometrics Gemini instrument (Norcross, Georgia), sample degassed at 200°C in vacuum for 12 h and measurements were made. For calculating the surface area parameters Physi View Calc tool, Micrometrics, Georgia was used to fit the data obtained.

2.3. *In vitro* Drug Loading And Delivery Studies

The typical drug loading and *in vitro* drug release experiments were performed as follows: Bioglass fibers were added to hexane solution in the ration of 1 g/50 mL with an ibuprofen concentration of 40 mg/mL. Similarly, Bioglass fibers were added in 1 g/10 mL of ciprofloxacin in the concentration of 40 mg/mL diluted in water. These suspensions were sealed and continuously shaken at 37°C for one day. The drug loaded sample was separated from the solution and dried in oven at 60°C. The hexane solution with ibuprofen before fiber loading and after fiber loading was observed with UV for testing the drug loaded concentration in the fibers. The drug loaded fibers were immersed into 100 mL phosphate buffer saline (PBS, pH 7.4) at 37°C with constant shaking (140 rpm).The shaking device was a desk-type constant-temperature oscillator (Rivotek, India). The drug release medium (2 mL) was withdrawn for analysis by UV-Vis absorption spectroscopy at a wavelength of 263 nm and 271 nm for ibuprofen and ciprofloxacin, respectively, at given time intervals and replaced with the same volume of fresh preheated PBS (37°C). The concentration of the released drug was estimated from the calibration graph. The experiments were performed in triplicate.

2.4. *In vitro* Biomineralization studies

In order to understand the biocompatibility and biomineralization of the Bioglass fibers, it was immersed in Hank's SBF solution (ASTM F2129-08), prepared using analytical grade chemicals and double distilled water, the solution similar to the solution used for corrosion studies for 28 days. The procedure for immersion was followed as prescribed by Kokubo et al.[12] After 7 and 14 days, the immersed samples were dried overnight at 80°C. The change in surface morphology of the samples was observed from FESEM and the elemental confirmation was observed from EDS. The phosphate formation was further confirmed from micro-Raman spectroscopy.

3. Results and Discussion

3.1. Optimization of processing parameters

The polymer solution and its viscosity play a significant influence in the electrospinning process. Hence the influence of the viscosity of the polymer wt% on the spinning process was analyzed first. PVP with 2 wt%, 4 wt%, 8 wt% and 10 wt% were tried for obtaining fiber formation. However, the fiber was formed only for 10 wt% below which only droplet formation has occurred even with variable applied voltages. The distance and the needle tip and the target were optimized to be at 12 cm for maximum receiving of fibers. With these two parameters kept as constant, other parameters such as feeding rate and applied voltage have been varied in the next conditions.

Since the transparent solution is highly viscous and the yield of the fiber was very low, the solvent such as ethanol and water is mixed to the transparent solution. Table S2 shows the

parameters with variation of the ethanol and water as diluting media. The feeding rate of 0.2 mL/h and 0.3 mL/h were varied at the applied voltage of 10 kV and 15 kV each respectively.

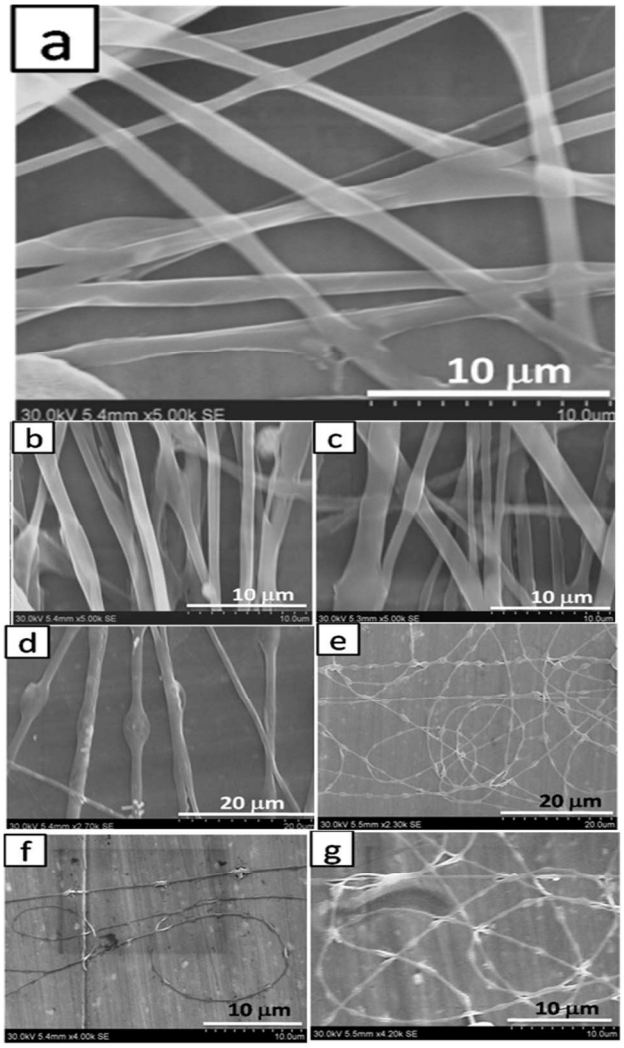

Fig. 1 Electrospun Bioglass fibers obtained at different processing conditions. (a) 0.3 mL/h and 10 kV (Ethanol dilution); (b) 0.3 mL/h and 15 kV (Ethanol dilution); (c) 0.2 mL/h and 10 kV (Ethanol dilution); (d) 0.2 mL/h and 15 kV (Ethanol dilution); (e) 0.3 mL/h and 15 kV (water dilution); (f) 0.2 mL/h and 10 kV (water dilution); (g) 0.2 mL/h and 15 kV (water dilution).

Figure 1 shows the morphology of fibers that were obtained with different feeding rates and applied voltage conditions. Bioglass fibers obtained at the feed rate of 0.3 mL/h and the applied voltage of 10 kV (Figure 1a) forms long elongated fibers with average diameter of 985 nm. While increasing the voltage to 15 kV, the fibers radius decreased to ~920 nm (Figure 1b). Whereas, with a decrease in the feed rate of 0.2 mL/h, the fibers became flat at 10 kV (Figure 1c) and bead formation also occurred at 15 kV (Figure 1d). With ethanol dilution condition, the fibers were collected using the drum collector for water dilution the extrusion of the fiber became narrow down and it was not possible to collect them using the drum collector, hence a plate collector was used. The water dilution fiber shows a smaller diameter twisted fiber morphology with lots of beaded structure. Bioglass fibers obtained at the feed rate of 0.3 mL/h and the applied voltage of 15 kV (Figure 1e) show an average diameter of 170 nm – 180 nm and each bead size is around 850 nm – 1000 nm. There occurs a large gap between the beads of the fiber. On decreasing the feed rate to 0.2 mL/h at 10 kV, average diameter increases to 190 nm – 200 nm and bead size decreases to 850 nm – 900 nm. However, with a further increase in the voltage both the diameter and bead size increase to 220 nm – 240 nm and 820 nm – 950 nm respectively.

3.2. Morphological evidence of porous Bioglass fibers

Fibers were fabricated by varying the parameters, by changing the dilution of the stock solution using ethanol, water and E+H with constant feed rate as 0.3 mL/h and constant voltage of 15 kV. The fibers obtained were sintered at 600 for 2 h. The morphology of the samples after sintered was imaged by FESEM (Figure 2a–c). Figure 2a shows the Bioglass fibers obtained using ethanol as the diluting media. It was obtained using the drum collector and hence the fibers were linear and parallel with each other. In the case of dilution with water, it was very difficult to collect the fiber using the drum collector and hence it was collected using a plate collector. Figure 2b shows the fibers obtained by using E+H as diluting media which yielded well compact dense nanofibers after sintering. The yield of these fibers was also very high. The beaded Bioglass fibers obtained using water dilutions that have been completely transformed into crystalline form after sintering (Figure 2c). The individual fiber and bead morphology are shown as insets in the respective figures.

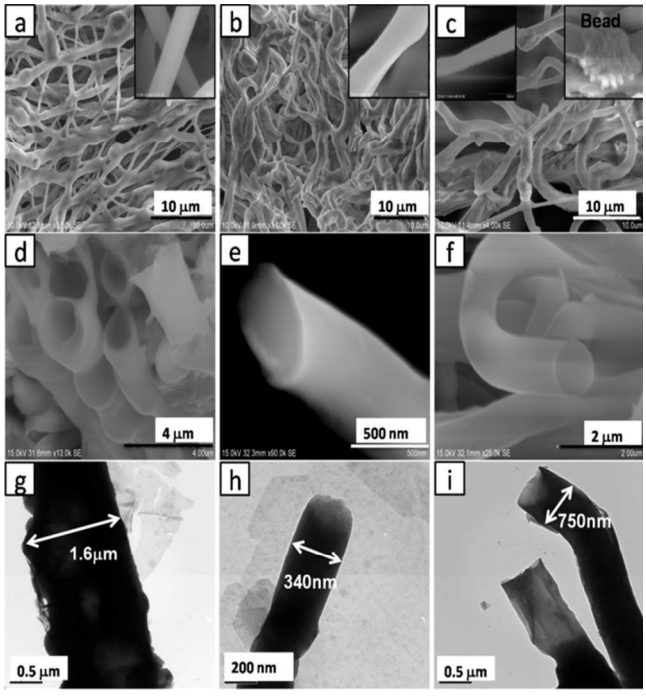

Fig. 2 FESEM top surface of (a) ethanol, (b) E+H, (c) water dilution; FESEM crossection view of (d) ethanol, (e) E+H and (f) water dilution;TEM images of (e) ethanol, (h) E+H and (i) water dilution prepared fibers.

3.3. Shell thickness variation with respect to dilution

The transectional and tranmission morphology of the fibers prepared in various dilutions are shown in Figure 2 (d –i). The images show that the fibers were hollow and the TEM images further confimed the shell thickness variation by increasing the transparency of the fibers (in figure 2 (g – i)). The mechanism of the formation of hollow fibers is schematically illustrated in Figure 3. In general, the formations of these hollow structures have been seemingly controlled by the competition between the phase separation dynamics and the solvent evaporation rate.[13] The fiber appears porous as the solvent-rich phase is dried out. It has been reported that the formation of porous fiber during electrospinning into the dry air environment is seemingly governed by solvent evaporation rate and phase separation kinetics.[14]

These processes are closely related to the equilibrium phase diagram of the polymer – solvent system in physical cooling (Figure 3a).[15] During the course of solvent evaporation, at a given temperature, the polymer concentration increases while passing through the co-existence regions such as metastable nucleation, growth regime and unstable spinodal regions. In the present case, during the electrospinning process, the solvent evaporation is taking place exclusively from the boundary and thus the concentration fluctuations develop "outside in," resulting in the skin – core morphology, i.e., hollow fibers. The dynamics of solvent escape across the boundary is expressed by Fick's second law of diffusion,

$$\frac{\partial \phi}{\partial t} = D\frac{\partial^2 \phi}{\partial x^2} \qquad (1)$$

where, ϕ is the concentration with dimensions of [mol/m], t is time [s], D is the diffusion coefficient with dimensions of [m/s] and x is the position, [m].[16] For variation in the fiber morphology, temperature is also another factor; however the electrospun was done in a closed environmental condition and the humidity was maintained constant throughout the experiment.

Hence, from the above, it is clearly shows that solvent evaporation was directly related to the fiber morphology. Dayal and Kyu also showed that solvent evaporation is linearly related to the shell thickness.[13] Here we used ethanol, water and ethanol+water dilution. The evaporation rate of these solvents is directly related to the surface tension of the solvents. Gonzalo et al. discussed the decrease in the surface tension of ethanol with an increase in the water ratio. At 30°C, the surface tension of ethanol (100%), E+H (50:50) and water (100%) are given as 71.21 $mN.m^{-1}$, 27.53 $mN.m^{-1}$ and 21.41 $mN.m^{-1}$ respectively.[17] Hence decrease in the dilution, led to a decrease the surface tension and thus the viscosity and evaporation rate also decreased. Accordingly, for ethanol diluted samples, the shell thickness is high and with an increase in the water dilution, the shell thickness decreases. This also leads to the earlier spindling of the fibers and bead formation at water dilution as shown in Figure 3.

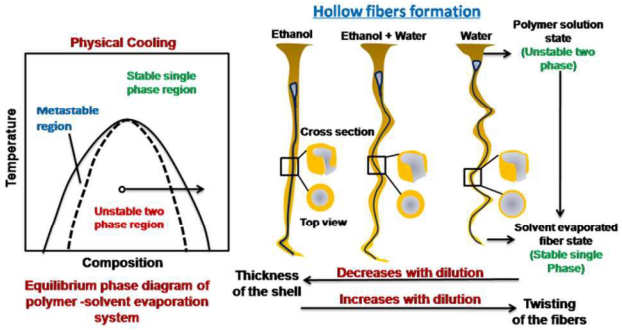

Fig. 3 Phase diagram of polymer - solvent evaporation phase diagram shows the unstable two phase region and the stable single phase region transformation, which was observed in fiber formation from the jet (two phase region) to tail (single stable region). The hollow fiber formation schematics show that an increase in dilution using water, leads to an increase in twisting of fibers and a decrease in thickness of the shell.

3.4. Phase and elemental confirmation of Bioglass 45S5 fibers system

Figure 4a shows the FTIR spectra of Bioglass prepared with different dilution conditions. The spectra are characterized by a very broad OH absorption band centred around 3424 cm and a weakly absorbed water band at 1650 cm^{-1}. Two other absorption bands observed at 926 cm^{-1} and 1024 cm^{-1} correspond to an asymmetric Si – O – Si stretching vibration of silanol groups. The peak centred at 565 cm^{-1} can be attributed to the P – O bond in crystalline phosphates. Similarly, the weak peak at 1212 cm^{-1} is attributed to the characteristic vibration of P = O bonds. Furthermore, the broad band centred at 1440 cm^{-1} is diagnostic of the vibrations of non – bridging PO_2 in PO_4^{3-} groups or CO_3^{2-} originated from a air during the sol-gel fabrication.[18] The vibrational modes obtained for the Bioglass fibers were comparable with those of biomorphic 45S5 Bioglass scaffold. The number of non – bridging oxygen (NBO) linked to Si increases the band at 926 cm^{-1} which was observed for ethanol dilution prepared fibers.[19]

The major features of the Raman spectra of the Bioglass were associated with bands of asymmetric and symmetric stretching vibrations of the silica network in the region 850 cm^{-1} – 1200 cm^{-1}. The spectra of the Bioglass fibers obtained by using different dilution media are given in Figure 4b. The Q_n species gave evidence for the presence of P – O bonds in addition to the Si – O – Si matrix. It can be seen that the spectral structures of Bioglass fibers are dominated by the high intensity Q_n unit at 939 cm^{-1}, which represents chains of metasilicates ($Si_2O_6^{2-}$) and high abundance of this species is a characteristic of highly bioactive glasses. The band situated at 1090 cm^{-1} is attributed to the stretching vibration of Si – O^- bonds in the $Q_3(Si_2O_5^{2-})$ tetrahedral units. The Q_2 and Q_3 bands are high and narrow for ethanol and E+H prepared fibers respectively. There also exists a strong band at 966 cm^{-1} that is due to the superposition of Si – O^- stretching vibrations in silicate tetrahedral units with two non-bridging oxygen atoms (Q_2 units) with the P – O^- stretching vibrations of PO_4 tetrahedra at 1040 cm^{-1} . A strong band is also observed at 437

cm^{-1} and is considered to arise from the rocking motion of the bridging oxygen atoms perpendicularly to the P – O – P plane. The P – O asymmetric peak at 565 cm^{-1} corresponds to bending vibrations in the PO tetrahedra.[20] All these bands confirm the formation of Bioglass 45S5 system.

Figure 4(c) shows the XRD spectra of the Bioglass fibers obtained by different dilution conditions and sintered at 600°C for 2 h. The spectra obtained were of low intensity , which shows the amorphous nature of the fibers formed and they were partially crystalline at some region giving the resultant XRD peaks. The peaks of fibers obtained using ethanol and water dilution media were similar to calcium hydroxyl carbonate (JCPDS No. 19 – 0272) and for E+H dilution, it was well matched with (JCPDS No. 84 – 0655). These two phases were proven to be highly biocompatible and commercially used in bone regeneration applications.[21-22] However, the usual crystal system was not observed in this fiber system which led us to further confirmation using XPS.

XPS survey spectrum (Figure 4d) identified carbon, calcium, silicon, sodium and the phosphorus constituents in the fabricated Bioglass fibers. The presence of sodium was confirmed from both the Na 1s core peak and Na KLL Auger peak. The Ca 2p doublet separation was clearly visible in water dilution prepared fibers. The carbon C 1s peak decreased with dilution. This is due to the presence of ethanol content in the solvent solution. During solvent-evaporation mechanism, the polymer content reaches the shell surface and higher shell thickness of ethanol prepared scaffolds contains higher carbon content. XPS was the tool which can measure up to the thickness of 10 atomic layers on the surface.[23] This result is in good correlation with the fiber formation mechanism discussed above.

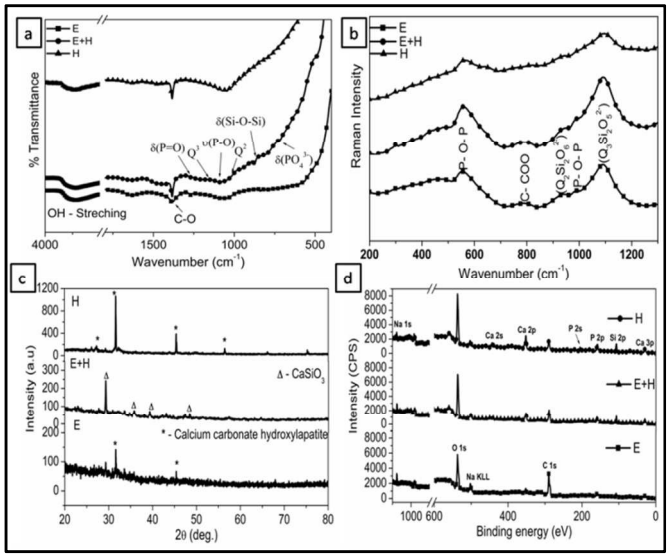

Fig. 4 (a) FTIR spectra of Bioglass 45S5 prepared under different dilution conditions; (b) Micro- Raman spectra of the Bioglass prepared using different dilution media, confirm the formation of Bioglass 45S5; (c) XRD spectra of Bioglass fibers obtained using different dilution conditions; (d) XPS survey spectra of Bioglass fibers obtained by different dilution conditions.

3.5. Surface area analysis of Bioglass fibers

The Brunauer-Emmet-Teller BET surface areas of all materials were calculated from the nitrogen and argon isotherms (Figure S4). The BET surface area analyses were obtained using the consistency criteria. The Brunauer-Emmet-Teller (BET) equation is given as

$$\frac{1}{Q[(P_0/P)-1]} = \frac{1}{X_m C} + \frac{C-1}{X_m C}\frac{P}{P_0} \qquad (2)$$

Using this equation and information from the isotherm, the surface area of the sample was measured. Here, Q is the weight of the nitrogen adsorbed at the given relative pressure, (P/P_0), X_m is monolayer capacity, which is the volume of gas adsorbed at standard temperature and pressure (STP), and C is a constant.[24]

The parameters (specific surface area is area per unit mass; specific pore volume is volume per unit mass) obtained were given in Table S3. The results show that a decrease in an increase trend for variation in dilution of the samples from ethanol, E+H and water prepared fibers. However, the occurrence of an increase and decrease in the pore volume is due to the presence of non – open pores of lengthened fiber formation in the beaded structure through water diluted samples. According to IUPAC; pores with the diameter greater than 50 nm were termed as macroporous materials,[25] we confirmed that our fibers were macroporous and will be suitable candidates for drug delivery applications.

3.6. *In vitro* Biomineralization and degradation of Bioglass fibers

The heat treated nanofibers were subsequently incubated in a SBF to examine their bioactivity by determining whether they induce the precipitation of bone like minerals on the surface.

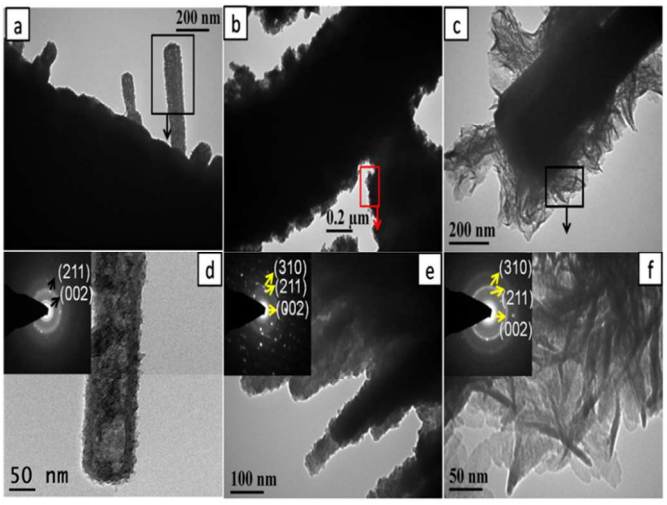

Fig. 5 *In vitro* immersion studies of Bioglass fibers obtained under different dilution conditions for 3rd day ((a) ethanol, (b) ethanol +water and (c) water) and the magnified images ((d) ethanol, (e) E+H and (f) water)

After 3 day of incubation, the surface of the fibers shows some elongated crystals on the surface using HRSTEM (Figure 5). At a higher magnification, it visibly shows the crystal formation on the surface of fibers with sizes of few tens of nanometre. The SAED pattern of the crystals further confirms the presence of diffuse diffraction rings in which the interplanar spacing agreed with those of an apatite-like crystal of (310), (211) strong and (002) weak rings.

Presumably the formation of the enamel-like HCA mesocrystals is due to the side-by-side assembly of the needle-like HCA crystals along their c-axis. The formation process of HCA on the fiber, surface that is from the emergence of spherical particles transiting to the formation of needle-like HCA mesocrystals, is well consistent with that reported by Vallet-Regi, but the crystallization of HCA is far faster.[26]

3.7. Drug loading and *in vitro* drug release kinetics

We investigated the drug loading and release performances of the Bioglass hollow fibers with two different drug carriers, such as ciprofloxacin and ibuprofen anti – inflammatory drugs. UV – Vis absorption spectra of the hexane, water solution containing ibuprofen, ciprofloxacin before and after drug loading were used to evaluate the drug loading capacity of porous hollow Bioglass fibers. [28-31] As shown in Figure 6(a), one can see that the absorption spectra of ciprofloxacin in the water show the characteristic peak at 275 nm[27] and ibuprofen in hexane solution show the characteristic peak of ibuprofen at 263 nm. On the basis of the calculation from the standard concentration curve, the ibuprofen loaded percentage (concentration from the molar absorptivity,ε = 440 $M^{-1}cm^{-1}$) was about 15 % (0.17 mg), 11.1% (0.13 mg), and 10.9% (0.12 mg) for ethanol, ethanol + water, and water prepared fibers with respect to the before loading condition 100% (1.13 mg) respectively. Similarly, for ciprofloxacin, with the molar absorptivity, ε = 30614 $M^{-1}cm^{-1}$ it was about 4.5% (1.97 μg), 2.3% (1 μg), and 0.95% (0.42 μg) for ethanol, ethanol + water, and water prepared fibers with respect to the before loading condition 100% (43.8 μg) respectively. From these results, E+H scaffold drug release behaviour was taken for further studies.

The change in the contrary of this variation in the amount of drug loaded in samples was directly proportional to the length of the Bioglass fibers. Youliang et al.[32] suggested that although both mesopores and hollow cores are main drug loading sites, the hollow cores should be the dominating ones to host the drug. From our interpretation of experimental observations fibrous length only influences the drug hosting of the fibers. The earlier report suggested that when the fibrous length is more than 30 mm, can the hollow cores become the sites for drug loading. In our present studies, even though ethanol prepared fibers show long fibrous length, the flaw in the fibers shell decreases the drug loading capacity.

The drug release kinetics of the ciprofloxacin and ibuprofen loaded Bioglass fibers (E+H) were investigated using the Higuchi model.[33] It is well acknowledged that the Higuchi equation ($C = K_H \sqrt{t}$) can very well describe the kinetics of the drug release from the carrier by a diffusion process through a linear relationship between the cumulative amount of released drug (C) and the square root of the release time (t). Figure 6a displays the drug release behaviour of ciprofloxacin in the 0.15 M NaCl medium which shows sustained drug release behaviour over a period of 6 h. The ciprofloxacin did not completely release, reaching a plateau of 70% drug release after 6 h. This shows a slow release over a period of time, which may be due to the relatively strong interaction between ibuprofen molecules and the fiber drug carrier. The inset of Figure 6b shows the relation between the cumulative amount of drug released and the square root of the release time of ciprofloxacin loaded Bioglass fiber (E+H) showing a good linear relationship with the square root of release time in 0.15 M NaCl and a correlation coefficient (R^2) of 0.998.

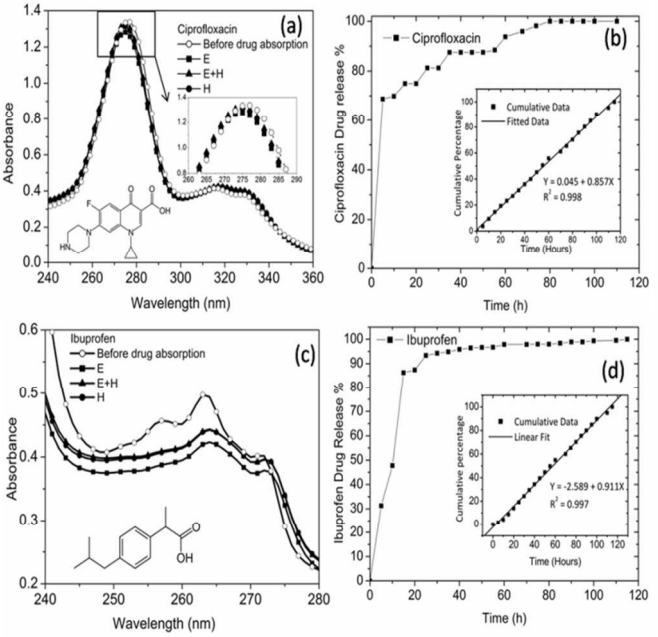

Fig. 6 (a) UV- Vis absorption spectra of water containing ciprofloxacin before and after ciprofloxacin loading in Bioglass fibers; (b) Cumulative release profile of ciprofloxacin in 0.5 M NaCl solution; (c) UV- Vis absorption spectra of hexane containing ibuprofen before and after ciprofloxacin loading in Bioglass fibers; (d) Cumulative release profile of ciprofloxacin in PBS solution. The inset of the drug release graph shows the cumulative drug release percentage as a function of the square root of the release time.

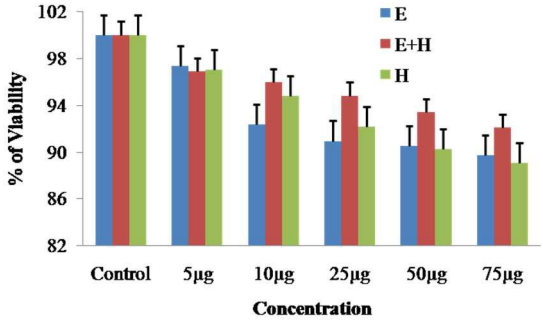

Fig. 7 Cell viability of the Bioglass fibers with MC3T3-E1 pre-osteoblast cell line.

The drug release behaviour of ibuprofen in PBS medium shows sustained drug release behaviour with 85% drug release over a period of 18 h as shown in Figure 6d. After 20 h, it has reached a steady plateau region, the cumulative drug release curve, which is given as the inset of Figure 6d.This shows a good linear relationship with the square root of release time in PBS and a correlation coefficient (R^2) of 0.997. Both the drugs confirm the drug delivery system governed by the diffusion process. The ciprofloxacin shows lesser sustain and prolonged drug release compare to ibuprofen, which is due to the F^- ions interaction in the ciprofloxacin with Ca^{2+} of Bioglass molecule.[33] 3.8 Cell viability using MTT assay

The cytotoxicity tests of the Bioglass hollow fibers were performed MC3T3–E1 pre–osteoblast cell line. The MTT assay showed no appreciable toxicity when the cells were co-cultured with Bioglass hollow fibers at concentrations in the range 5µg/mL – 75 µg/mL (Figure 7)). All the samples showed good cell viability and it is noted that dense fibrous arrangement of fibers prepared using E+H dilution provides higher cell viability. According to Biological Evaluation of medical devices – Part 5: Tests for *in vitro* cytotoxicity (ISO 10993 – 5: 2009), if the cell viability of the material is less than 70%, then it has a cytotoxic potential.[33] However, all the Bioglass fibers exhibit the cell viability that is greater than 90%, indicating that the as-synthesized samples are biocompatible with pre-osteoblasts cell lines and are suitable for *in vivo* applications.

4. Conclusion

In summary, the optimized conditions for obtaining hollow Bioglass fibers were achieved in the electrospinning technique. The rapid solvent evaporation during electrospinning and phase separation between the PVP polymer and the solvent play the essential roles in the formation of hollow cores in the Bioglass fibers. The viscosity of the Bioglass sol was varied by diluting with ethanol and water in different ratios and we conclude that the presence of water alters the pore diameter of the fiber. Three different fibers were obtained by varying the dilution of ethanol-water, the essential phase, and the functional and morphological confirmations for the formation of Bioglass in the fiber structure. When the fabricated fibers subjected to immersion studies in SBF, there occurs the formation of needle HCA growth on the *c*-axis similar to the bone on the 3rd day itself. Further, it shows the complete covering of Bioglass fibers with apatite formation on the 7th day of the sample prepared using ethanol and water in the ratio of 1:1. The hollow fibers show good drug loading and releasing kinetics with the sustained release of 70% and 85% for ciprofloxacin and ibuprofen samples with the releasing time of 6 h and 18 h respectively. This suggests that the hollow fibers will be highly suitable for drug delivery and wound healing applications. Since the fibers were well organized in 3D macroporous structure at the macroporous scale with high biocompatibility; it has the potential applications in wound and hard tissue repair applications.

Acknowledgements

One of the authors, D. Durgalakshmi, would like to acknowledge Lady Tata Memorial Trust, Mumbai for providing the Junior and senior fellowships for carrying out this research work. All the authors would greatly acknowledge the NCNSNT instrumentation facilities funded by UGC-MHRD, New Delhi, India.

Notes and references

[a]National Centre for Nanoscience and Nanotechnology, University of Madras, Guindy campus, Chennai 600025, India.
Fax: 044-22352494/22353309; Tel: 044-22202749
*E-mail: balasuga@yahoo.com

Electronic Supplementary Information (ESI) available: Schematic representation of the fabrication of Bioglass fibers using the electrospinning technique, Optimization conditions of the Bioglass fibers and the inference obtained at different processing conditions, Porosity analysis of Bioglass fibers, BET multipoint surface area analysis of the Bioglass fibers, *In vitro* immersion studies of Bioglass fibers obtained under different dilution conditions for 7th day and Micro-Raman studies of Bioglass fibers immersed in simulated body fluid solution after 7 day and 14 day.

[1] E. M. Christenson, K. S. Anseth, J. J. J. P. van den Beucken, C. K. Chan, B. Ercan, J. A. Jansen, C. T. Laurencin, W. J. Li, R. Murugan, L. S. Nair, *J. Orthop. Res.,* 2007, **25**, 11.
[2] V. Karageorgiou, D. Kaplan, *Biomaterials,* 2005, **26**, 5474.
[3] F. Guilak, D. L. Butler, S. A. Goldstein, F. Baaijens, *J. Biomech.,* 2014.
[4] E. K. F. Yim, K. W. Leong, *Nanomedicine: Nanotechnology, Biology and Medicine,* 2005, **1**, 10.
[5] (a) L. L. Hench, *J. Mater. Sci. Mater. Med.*, 2006, **17**, 967. (b) D. Durgalakshmi., and S. Balakumar, *Phys. Chem. Chem. Phys*., 2015, **17**, 1247.
[6] B. Dhandayuthapani, Y. Yoshida, T. Maekawa, D. S. Kumar, *Int. J. Polymer Sci.,* 2011, .
[7] S. Patel, K. Kurpinski, R. Quigley, H. Gao, B. S. Hsiao, M.-M. Poo, S. Li, *Nano Lett*., 2007, **7**, 2122.
[8] J. R. Jones, *Acta Biomater,* 2013, **9**, 4457.
[9] M. N. Rahaman, D. E. Day, B. Sonny Bal, Q. Fu, S. B. Jung, L. F. Bonewald, A. P. Tomsia, , *Acta Biomater,* 2011, **7**, 2355.
[10] H. Lu, T. Zhang, X. P. Wang, Q. F. Fang, *J. Mater. Sci. Mater. Med.,* 2009, **20**, 793.
[11] X. Yan, X. Huang, C. Yu, H. Deng, Y. Wang, Z. Zhang, S. Qiao, G. Lu, D. Zhao, *Biomaterials,* 2006, **27**, 3396.
[12]T. Kokubo, H. Takadama, *Biomaterials,* 2006, **27**, 2907.
[13] P. Dayal, T. Kyu, *J. Appl. Phys.,* 2006, **100**, 043512.
[14] P. Dayal, J. Liu, S. Kumar, T. Kyu, *Macromolecules,* 2007, **40**, 7689.
[15] K. Nakanishi, N. Tanaka, *Acc. Chem. Res.,* 2007, **40**, 863.
[16] L. Mejlbro, *Durability of Concrete in Saline Environment. Proceedings. P. Sandberg (Ed.) Lund,* 1996, 127.
[17] G. Vazquez, E. Alvarez, J. M. Navaza, *J. Chem. Eng. Data,* 1995, **40**, 611.
[18] D. Carta, J. C. Knowles, M. E. Smith, R. J. Newport, *J. Non-Cryst. Solids,* 2007, **353**, 1141.

[19] A. R. Boccaccini, Q. Chen, L. Lefebvre, L. Gremillard, J. Chevalier, *Farad. Discuss,* 2007, **136**, 27.
[20] J. Kwiatkowska, K. Suchanek, B. Rajchel, *Acta. Phys. Pol. A*, 2012, **121**, 502.
[21] R. A. Yukna, C. N. Yukna, *J. Clin. Periodontol.,* 1998, **25**, 1036.
[22] S. Xu, K. Lin, Z. Wang, J. Chang, L. Wang, J. Lu, C. Ning, *Biomaterials,* 2008, **29**, 2588.
[23] M. Cerruti, C. L. Bianchi, F. Bonino, A. Damin, A. Perardi, C. Morterra, *J. Phys. Chem. B,* 2005, **109**, 14496.
[24] S. Brunauer, P. H. Emmett, E. Teller, *J. Am. Chem. Soc.,* 1938, **60**, 309.
[25] Z. Ryu, J. Zheng, M. Wang, B. Zhang, *Carbon,* 1999, **37**, 1257.
[26] M. Vallet-Regí, C. V. Ragel, Antonio J. Salinas, *Eur. J. Inorg. Chem.,* 2003, **2003**, 1029.
[27] J. Duan, Z. Yuan, *J. Agri. Food. Chem.*, 2001, **49(3)**, 1087.
[28] R. K. Singh, D. P. Kapil, J. J Kim et al., *ACS Appl. Mater. Inter.*, 2014, **6**, 2201.
[29] S. Kwon, R. K. Singh, T. H. Kim et al., *Acta Biomater.*, 2014, **10(3),** 1431.
[30] R.K. Singh, T.H. Kim, J. J. Lee et al., *RSC Adv.*, 2013, **3(23)**, 8692.
[31] R.K. Singh, G. Z. Jin, C. Mahapatra, *ACS Appl. Mater. Inter.*, 2015, **7(15)**, 8088.
[32]Y. Hong, X. Chen, X. Jing, H. Fan, Z. Gu, X. Zhang, *Adv. Funct. Mater.,* 2010, **20**, 1503.
[33] G. S. Kumar, R. Govindan, E. K. Girija, *J. Mater. Chem. B,* 2014, **2**, 5052.

